Benjamin Besser, Saad Malik, Michael Baune, Stephen Kroll, Jorg Thöming,
Kurosch Rezwan

The influence of the functional group density on gas flow and selectivity: Nanoscale interactions in alkyl-functionalized mesoporous membranes

Journal Article as: peer-reviewed accepted version (Postprint)

DOI of this document*(secondary publication): 10.26092/elib/2485

Publication date of this document: 18/09/2023

* for better findability or for reliable citation

Recommended Citation (primary publication/Version of Record) incl. DOI:

Benjamin Besser, Saad Malik, Michael Baune, Stephen Kroll, Jorg Thöming, Kurosch Rezwan,
The influence of the functional group density on gas flow and selectivity: Nanoscale interactions in alkyl-functionalized mesoporous membranes, Microporous and Mesoporous Materials, Volume 237, 2017, Pages 38-48, ISSN 1387-1811,
https://doi.org/10.1016/j.micromeso.2016.09.026

The influence of the functional group density on gas flow and selectivity: Nanoscale interactions in alkyl-functionalized mesoporous membranes

Benjamin Besser [a], Saad Malik [a], Michael Baune [b], Stephen Kroll [a, c, *], Jorg Thöming [b, c], Kurosch Rezwan [a, c]

[a] Advanced Ceramics, University of Bremen, Am Biologischen Garten 2, 28359 Bremen, Germany
[b] Center for Environmental Research and Sustainable Technology (UFT), University of Bremen, Leobener Strasse 1, 28359 Bremen, Germany
[c] Centre for Materials and Processes (MAPEX), University of Bremen, Bibliothekstraße 1, 28359 Bremen, Germany

ARTICLE INFO

Article history:
Received 29 July 2016
Received in revised form
2 September 2016
Accepted 14 September 2016
Available online 15 September 2016

Keywords:
Mesoporous ceramic membrane
Surface functionalization
Gas permeation
Knudsen diffusion

ABSTRACT

Mesoporous inorganic structures with mean pore diameters of 26 nm are prepared by extrusion based on a yttria stabilized zirconia nanopowder. The sintered capillary membranes serve as model structures to investigate the influence of an alkyl-chain (C_{16}) surface functionalization on the gas diffusion kinetics of argon (Ar), nitrogen (N_2) and carbon dioxide (CO_2) in mesopores. The density of the C_{16} alkyl-chains immobilized on the membrane surface has an effect on both, gas flow as well as gas selectivity. For low functional group densities (<4 groups nm^{-2}), the gas flow is reduced without having an effect on the selectivity. In contrast, for high alkyl-chain densities (>4 groups nm^{-2}) the mean distance between the C_{16}-chains is reduced to the order of magnitude of the gas molecules leading to a reduction in gas flow and a significant change of the gas selectivity. The selectivity is found to be influenced depending on the molecular diameter of the gas species, being more evident for CO_2 compared to Ar and N_2, suggesting a separation mechanism more comparable to molecular sieving than to surface diffusion.

1. Introduction

Gas-solid interactions within porous materials are important for many processes and applications such as solid oxide fuel cells, catalysis, gas chromatography, gas separation or gas adsorption on solid sorbents [1–7]. The pore size of the material can be very different ranging from several micrometers to nanometers. Nevertheless, the performance of a process and its characteristics are often defined or driven by nanoscale interactions of gas molecules with the solid material surface, for example in the capillary of a gas chromatography column or at the pore walls of an inorganic membrane. Depending on the pore size and the Knudsen number (Kn), various transport mechanisms dominate inside the porous structures. Asymmetric inorganic membranes are a very good and well known example of porous materials where different transport mechanisms can occur simultaneously. They usually consist of a macroporous support structure (>50 nm, usually 1–10 μm), one or two mesoporous intermediate layers (10–50 nm) and a micro- or mesoporous top layer with pores <10 nm [8,9]. Determined by the structural proportions, the gas transport is dominated by viscous flow in the macropores of the support structure ($Kn > 1$), Knudsen diffusion in mesoporous intermediate layers ($Kn > 1$), and surface diffusion or molecular sieving in the top layer ($Kn > 10$) [10–16]. The transitions between the transport mechanisms are fluid, but under ambient pressure and room temperature (RT) viscous flow can be neglected in pores <50 nm and surface diffusion is negligible in pores >10 nm. In particular in gas chromatography as well as in membrane separation based on surface selective flow, the gas-wall interactions define the properties of the material [17–19]. Despite the difference in pore dimensions which are in the micrometer range for chromatography columns and in the nanometer range for membranes, in both cases the selective properties depend on the surface functionality. Therefore, different surface functionalization

* Corresponding author. Advanced Ceramics, University of Bremen, Am Biologischen Garten 2, 28359 Bremen, Germany.
E-mail address: stephen.kroll@uni-bremen.de (S. Kroll).

http://dx.doi.org/10.1016/j.micromeso.2016.09.026

strategies with numerous functional groups are used to alter the surface chemistry and influence the gas-solid interactions [4,20–22]. For example, alkyl-functionalizations have been successfully applied in both, chromatographic applications [23] as well as membrane separation [24–28]. Especially in membrane separation, it is often observed that the membrane flux is reduced by several orders of magnitude as a result of the surface functionalization, independent of functional group type [20–22,24–30]. Usually this is explained by the reduction in pore size and porosity due to the functional groups immobilized on the pore walls. Surprisingly, the decrease in pore size and porosity is seldom in the order of magnitude of the decrease in flux. This indicates that the full impact of surface functionalizations on the gas flow through a porous material has not been completely understood yet. Asymmetric membranes are often used for the investigation of surface functionalizations and their impact on gas flow properties. But, the total gas flow of the membrane will be a superposition of multiple transport phenomena, because they consist of multiple layers with pore sizes over several length scales. For this reason, asymmetric membranes are not the most favorable structures for the analysis of transport phenomena depending on surface functionality as well as pore size. To achieve fundamental understanding about nanoscale interactions of gas molecules with functional layers and their relations to pore size and porosity, the gas transport mechanisms need to be studied separately for each length scale. This study aims to experimentally investigate the impact of the surface functional group density on the gas diffusion dynamics in mesopores between 10 and 50 nm, where Knudsen diffusion is dominating. The study is focused on the experimental determination of the gas transport with high accuracy, without the development of analytical or semi-empirical gas transport models. For this purpose, mesoporous ceramic capillary membranes are prepared by an extrusion process using yttria stabilized zirconia nanopowder. These membranes serve as model structures which are functionalized in a second step with varying amounts of an alkyl-silane showing a C_{16}-chain as functional group (hexadecyltrimethoxysilane, HDTMS). All membranes are characterized concerning their pore size, open porosity, specific surface area and alkyl-chain density on the surface. Single gas permeation measurements using argon (Ar), nitrogen (N_2) and carbon dioxide (CO_2) are performed to investigate the impact of the functional group density on the gas diffusion kinetics within the mesoporous structures.

2. Experimental

2.1. Materials

The mesoporous ceramic structures are fabricated using a yttria (3 mol%) stabilized zirconia nanopowder (YSZ, primary particle size 30 nm, VP Zirkonoxid 3-YSZ, Lot. 3157061469) purchased from Evonik Industries, Germany. 3-aminopropyltriethoxysilane (APTES, ≥98%, product number A3648, Lot. WXBB5181V) and polyvinyl alcohol (PVA, fully hydrolyzed, product number P1763, Lot. SLBD2875V), used as additives, are obtained from Sigma-Aldrich Chemie GmbH, Germany. For the surface functionalization, sulfuric acid (H_2SO_4, 95–97%, product number 30743, Lot SZBF0330V) as well as hydrogen peroxide ((H_2O_2, ≥35%, product number 95299, Lot SZBE2740V) are provided from Sigma-Aldrich Chemie GmbH, Germany, whereas acetone (≥99%, product number 20063.365, Lot. 16E041994) is obtained from VWR International, Belgium, and hexadecyltrimethoxysilane (HDTMS, 90%, product number AB111166, Lot. 1270013) is purchased from ABCR, Germany. For all experiments, double deionized water with an electrical resistance of 18 MΩ (Synergy®, Millipore, Germany) is used. All materials are used as received and without further purification.

2.2. Processing and functionalization

2.2.1. Membrane preparation

Mesoporous membrane model structures are prepared based on an established extrusion process [31,32]. In short, using water as solvent (21 wt%), the YSZ nanopowder (79 wt%) is mixed with APTES (5 dwb.%) serving as dispersant as well as sintering additive and PVA (6 dwb.%) serving as temporary binder. All ingredients are mixed and homogenized using a planetary ball mill (PM400 from Retsch, Germany). Prior to milling, the PVA is dissolved in hot water (≈80 °C) using a microwave (MD14482 Studio, Medion, Germany) to ensure a homogeneous slurry and avoid membrane defects due to PVA granules. The preparation process is schematically shown in Fig. 1A. After mixing, the homogeneous slurry is shaped into capillaries using a self-made lab extruder with a 2 mm die and a 1 mm pin [33]. After drying the green bodies for 2 days at room temperature, the membranes are finally sintered for 2 h at 1050 °C (the sintering program is given in Ref. [34]).

2.2.2. Surface functionalization

To alter the surface chemistry of the membrane, the surface is functionalized with HDTMS (C_{16}-chain) molecules based on a wet chemical functionalization process [35]. The process consists of the surface activation by acidic hydroxylation followed by a chemical functionalization using the silane HDTMS as indicated in Fig 1B. The surface activation is carried out by immersing the membranes into freshly prepared Piranha solution (95–97% H_2SO_4:35% H_2O_2, 3:1, v/v). After 30 min of incubation the membranes are washed with double deionized water until reaching neutral pH and subsequently dried at 70 °C for 30 h. For the drying process, the membranes are placed in an open glass petri dish which is finall$_{0.15}$y put into a drying oven. It should be pointed out at this point, that it is of high importance for the functionalization process that all membranes are completely dry before continuing with the surface silanization. After successful drying of the membranes, the membranes are immersed into a HDTMS solution with an acetone-water mixture (95:5, v/v) as solvent. The surface functionalization is carried out by boiling under reflux for 16 h aiming at monolayer formation of HDTMS molecules. In this study, the HDTMS concentration of the solution is varied from 0.01 to 0.2 M to adjust the loading capacity of immobilized alkl-chains on the surface. Finally, the membranes are washed with acetone and dried for 2 h at 70 °C. The samples are named according to the HDTMS concentration of the stock solution used as subscript, namely $M_{0.01}$, $M_{0.05}$, $M_{0.1}$, $M_{0.125}$, M and $M_{0.2}$, samples without a surface functionalization are named M_{non-f}.

2.3. Membrane characterization

2.3.1. Structural characterization

Nitrogen adsorption/desorption measurements as well as thermogravimetric analysis (TGA) are carried out to obtain information about the porous membrane structure (i.e. pore size distribution, pore volume and porosity) and the functional group density of immobilized alkyl-chains per membrane surface area as schematically shown in Fig. 1C. Nitrogen adsorption measurements are performed at −196 °C using a BELSORP-mini II (Bel Japan Inc., Japan). Prior to the measurement, the samples are degassed at 120 °C for at least 3 h under reduced pressure (≤2 Pa) followed by cooling to RT under argon atmosphere. Based on the adsorption isotherms, the mesopore size distribution and mean pore diameter are determined according to the BJH-method [36]. Furthermore, the specific surface area is calculated according to BET-method [37] and the open porosity is obtained based on the true density determined by helium pycnometry (Pycnomatic ATC, Porotec, Germany). All measurements are performed three times to ensure

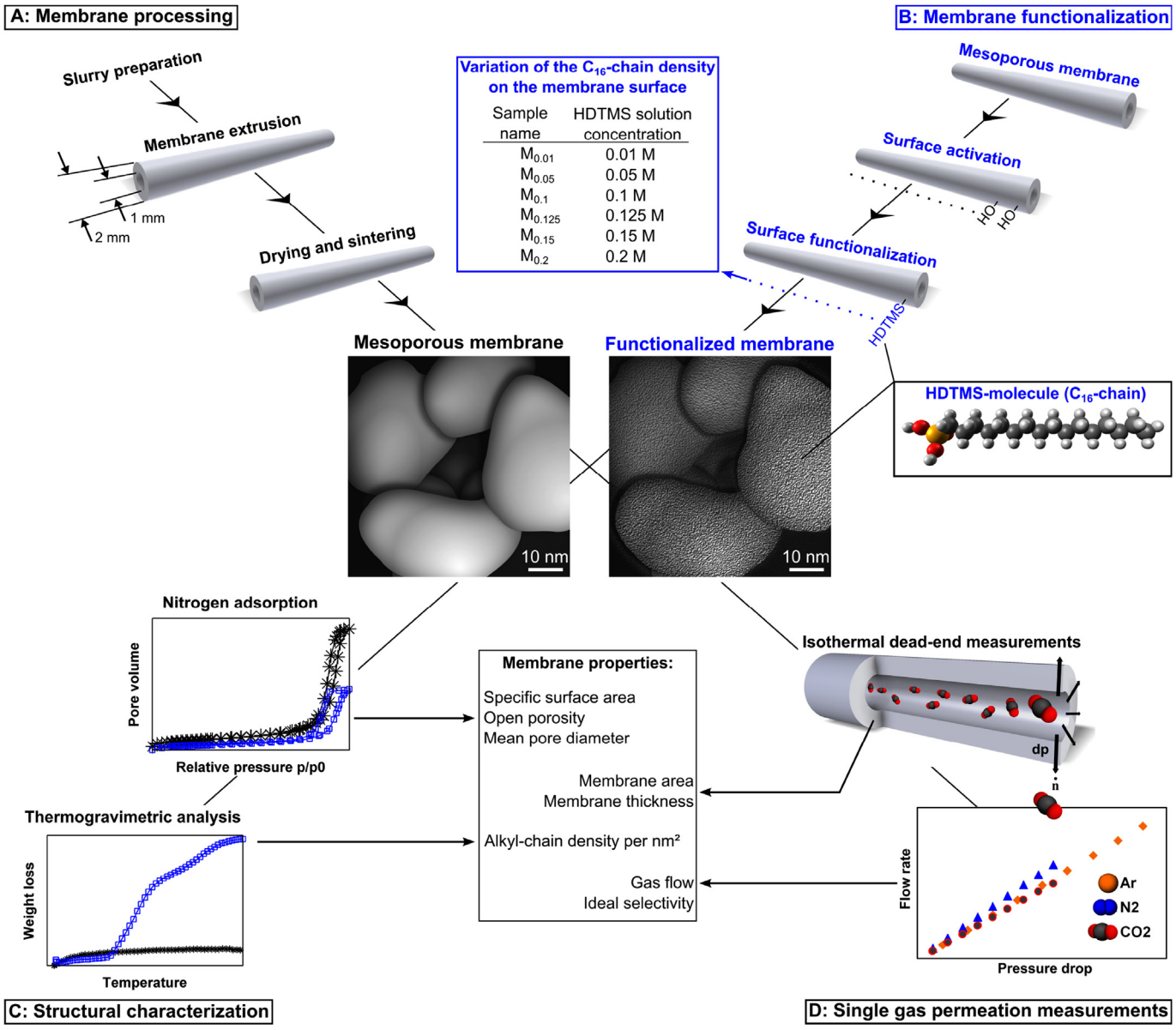

Fig. 1. Schematical overview over membrane preparation (A), membrane functionalization (B), structural characterization (C) and gas permeation measurements (D). The pictures of the membrane structures are modeled based on transmission electron microscopy images of the YSZ powder.

reproducibility. The amount of alkyl-chains on the surface is characterized by TGA as well as differential thermal analysis (DTA) using a STA503 (Bähr-Thermoanalyse GmbH, Germany). Between 70 and 100 mg of membrane sample is placed in a crucible and heated from 20 to 900 °C with a heating rate of 10 °C min^{-1} operating in air with a constant air flow rate of 10 L min^{-1}. All measurements are performed three times to ensure reproducibility. The quantitative analysis of the measurement data is performed similar to our previous study [30]. In short, it is assumed that the weight loss below 200 °C is predominantly caused by water desorption and the weight loss above 600 °C is not caused by organic decomposition. Therefore, the weight loss between 200 and 600 °C is taken into account to calculate the amount of immobilized alkyl-chains. For reference, the average weight loss of non-functionalized membranes between 200 and 600 °C is used. Furthermore, the final results are correlated with the specific surface area determined by nitrogen adsorption and the molecular mass of the organic compounds of an HDTMS molecule (ideally) covalently bound to the surface. For this, we assume that (ideally) all methoxy-groups of the HDTMS molecules (total, $C_{19}H_{42}O_3Si$) are reacted with the water molecules to form methanol which left the HDTMS in a hydrolyzed state ($C_{16}H_{36}O_3Si$, schematically illustrated in Fig. 2). This assumption is supported by observations in the lab when adding HDTMS to the solvent mixture. The HDTMS molecules will then condense in this state on the ceramic surface during the functionalization process. It is assumed that all atoms are degraded during the heating process except Si and O which form silica. Therefore we assume 229.5 g mol^{-1} ($C_{16}H_{36}$) as the molar mass of all degradable compounds of a HDTMS molecule covalently bound to the surface. The resulting values given in the number of alkyl-chains per membrane surface area are presented in groups nm^{-2} and further referred to as functional group density or alkyl(C_{16})-chain density.

2.3.2. Single gas permeation measurements

Gas permeation measurements are performed to investigate the influence of the functional group density on the gas transport of the

mesoporous structures analyzed in terms of gas flow and selectivity as indicated in Fig. 1D. Single gases, namely argon (Ar), nitrogen (N_2) and carbon dioxide (CO_2) are used with the system operating in dead-end mode [30,38]. The temperature is kept constant at 20 °C and the applied dead-end pressure is 80 kPa. In general, the dead-end pressure remains constant over the measurement time and non-stationary effects are considered negligible due to the very large dead-end volume compared to the total volume of the measurement system. Before integrating the membranes into the measurement system, they are heated for 3 h at 120 °C to desorb moisture. To ensure a high purity of the gas phase within the measurement system, the whole system is washed three times with the ongoing gas species by reducing the pressure to around 0.3 kPa and refilling to 160 kPa. Prior to measurement, the membrane sample is flushed with the used test gas for 1 min with a pressure difference of around 160 kPa. The measurements are performed by measuring the gas flow rate over nine different pressure drops applied over the membrane. After reaching steady state conditions, gas flow, pressure and temperature are averaged over 120 s. Each measurement is performed three times to ensure reproducibility. The results of the gas permeation measurements are analyzed in terms of ideal selectivity and gas flow in comparison to the Knudsen theory. Ideal selectivities $\alpha_{i,j}$ of gas i and j are obtained by linear regression of the flow rates against the pressure drop according to Equation (1).

$$\alpha_{i,j} = \frac{(\partial \dot{n}/\partial p)_i}{(\partial \dot{n}/\partial p)_j}. \tag{1}$$

According to the Knudsen theory, the molar flow $\dot{n}_{i,j}$ through a porous media with porosity ε, pore diameter d_{Pore} and tortuosity τ is directly proportional to the pressure drop Δp_i of a gas i possessing the molar mass M_i at a given temperature T (see Equation (2)).

$$\frac{\dot{n}_i}{A} = \frac{4\varepsilon d_{Pore}}{3\tau^2\sqrt{2\pi RTM_i}} \frac{\Delta p_i}{\delta}. \tag{2}$$

Here, R is the universal gas constant and A and δ represent membrane area and thickness, respectively. Following this equation and assuming constant temperature and pressure as well as similar gas and membrane properties, theoretical selectivities can be calculated as shown in Equation (3). These so called Knudsen selectivities are used as reference.

$$\alpha_{Kn,ij} = \sqrt{\frac{M_j}{M_i}}. \tag{3}$$

To analyze the gas flow of membranes possessing different densities of alkyl-chains, gas flow rate and pressure drop are recalculated to dimensionless terms using the relation for the Knudsen flow and the maximum applied pressure as given in Equation (4).

$$\frac{3\delta\dot{n}_i\sqrt{2\pi RTM_i}}{4A\varepsilon d_{Pore}} \frac{1}{p_{i,max}} = \frac{1}{\tau^2} \frac{\Delta p_i}{p_{i,max}}. \tag{4}$$

Here, the porosity (ε) and pore diameter (d_{Pore}) are obtained from nitrogen adsorption measurements and temperature (T), molar flow ($\dot{n}_i$) as well as pressure (p_i) are determined during the gas permeation measurements. The membrane wall thickness is determined by measuring the inner (d_{inner}) and the outer diameter (d_{outer}) in eight different directions at the membrane cross section using a digital microscope (VHX-600DSO, Keyence, Japan). The mean thickness is defined as $\delta = \frac{d_{outer} - d_{inner}}{2}$ using the mean inner and outer diameters. The membrane surface area is calculated using the mean outer diameter and the average length l of the capillary membrane measured from four sides using a micrometer table (Plμ 2300, Sensofar technology, Spain), where the mean membrane area is defined as $A = \pi d_{outer} l$.

2.3.3. Modeling of alkyl-chain distance

To theoretically analyze the functional group density, a simple modeling approach is used to calculate the mean distance between C_{16}-chains immobilized on the membrane surface as schematically shown in Fig. 2. For each iteration step, uniform and non-overlapping circles, each representing a single alkyl-chain, are distributed randomly over a circular region with the chosen radius of 10 nm representing an ideal fraction of the membrane surface area (see Fig. 2A). The number of circles depends on the desired C_{16}-chain density per membrane surface area. The diameter of the circles is chosen according to the kinetic diameter of methane to 380 p.m. [39], assuming a similar kinetic diameter along the C_{16}-chain. To exclude boundary effects, only the circles within a radius

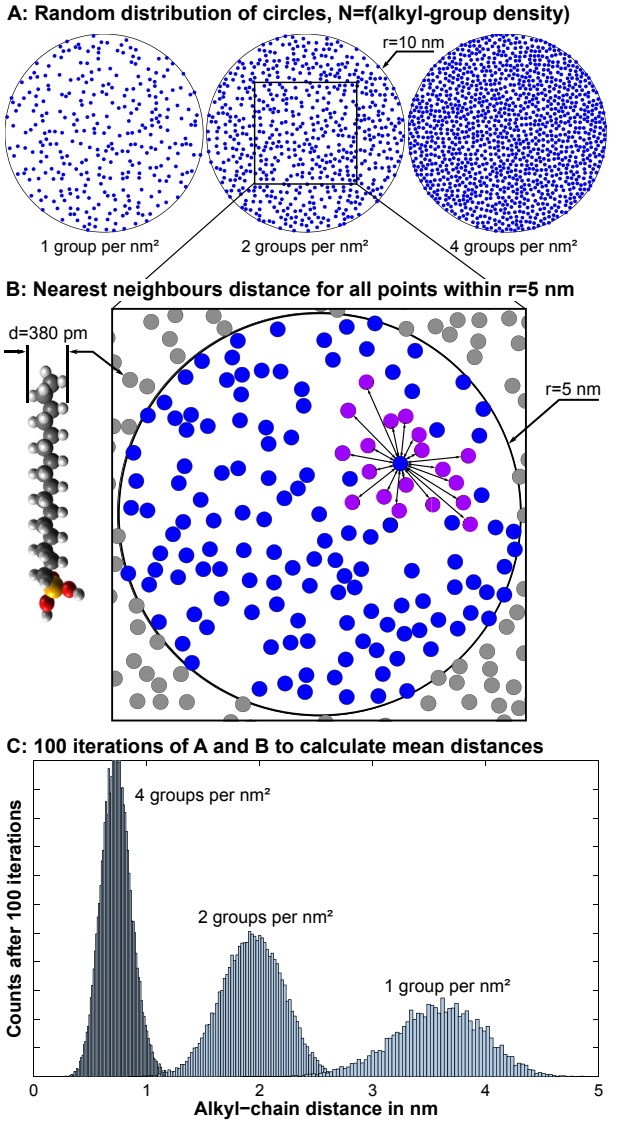

Fig. 2. Schematical overview of the model used to calculate the mean distance between C_{16}-chains. Nonoverlapping circles are randomly distributed within a radius r = 10 nm (A). For all circles within a r = 5 nm the distances to their nearest neighbors are calculated (B). After repeating the process for 100 iterations the data is statistically analyzed (C).

of 5 nm are used for further analysis. For each circle within this radius all nearest neighbors which are directly facing are determined and the distances are calculated (see Fig. 2B). This procedure, randomly distribution and determining all neighbor distances for all circles within 5 nm, is repeated 100 times for each chosen C_{16}-chain density to ensure a sufficient amount of data for a statistical distribution (see Fig. 2C). The results are presented in mean value and standard deviation using the distances from all considered circles in 100 iterations. Based on the experimental determination of the alkyl-chain density by TGA, functional group densities ranging from 0.1 to 4.4 groups per nm^2 with a step size of 0.1 are used for calculation.

3. Results

3.1. Structural characterization

Porous capillary membranes made of YSZ with a mono-modal pore size distribution are prepared by extrusion to serve as mesoporous model structures. To verify the pore structure, nitrogen adsorption/desorption measurements are performed. Fig. 3A shows exemplary nitrogen adsorption/desorption isotherms for membranes functionalized with varying C_{16}-chain concentrations (subscripts according to HDTMS concentration 0.01–0.2 M). All adsorption/desorption isotherms feature a hysteresis loop which can be classified as type IV according to IUPAC classification [40]. With increasing HDTMS concentration of the applied stock solution the total pore volume of the functionalized membranes decreases from 69.9 ± 4.8 ($M_{non-f.}$) to 42.1 ± 1.1 cm^3 (STP) g^{-1} ($M_{0.2}$). Following the Barrett–Joyner–Hallenda (BJH) model [36], Fig. 3B shows the corresponding incremental pore volume distributions depending on the pore diameter. All membranes show a similar, mono-modal pore size distribution with the maximum of incremental pore volume between 20 and 30 nm. The total mesopore volume (data not shown) is nearly identical with the total pore volume which indicates a pore structure solely consisting of mesopores. In addition, scanning electron microscopy images of the cross section of the membrane show a highly homogeneous pore network throughout the whole membrane thickness (data not shown).

In Table 1 the results for the structural analysis derived from nitrogen adsorption/desorption measurements are summarized. Following the trend indicated by the isotherms in Fig. 3A, both, the specific surface area as well as the open porosity decrease with increasing HDTMS concentration of the stock solution. Here, the decrease in specific surface area of 47% is higher than the reduction in open porosity, which decreases by 29% comparing $M_{non-f.}$ and $M_{0.2}$. Furthermore, the mean pore diameter determined by the BJH-method is reduced due to the C_{16}-functionalization from 26 nm to around 21 nm. It is especially noticeable, that the decrease in mean pore diameter is similar for all functionalized membranes ($M_{0.01}$ to $M_{0.2}$) and therefore independent from the HDTMS concentration in the stock solution as well as the correlating decrease in open porosity and specific surface area.

To analyze and quantify the amount of C_{16}-chains immobilized on the membrane surface depending on the HDTMS concentration of the applied stock solution, TGA/DTA measurements are carried out. Fig. 4 shows the TGA curves of exemplary measurements for the functionalized membranes with varying HDTMS concentrations ($M_{0.01}$ to $M_{0.2}$) in comparison to a non-functionalized membrane ($M_{non-f.}$) for a temperature ranging from room temperature (20 °C) to 650 C. $M_{non-f.}$ shows only a small weight loss (~0.5%), mostly below 200 °C (~0.4%). In turn, all C_{16}-functionalized membranes show little amount of weight loss up to 200 °C (~ 0.2%), which significantly increases when the temperature exceeds 200 °C

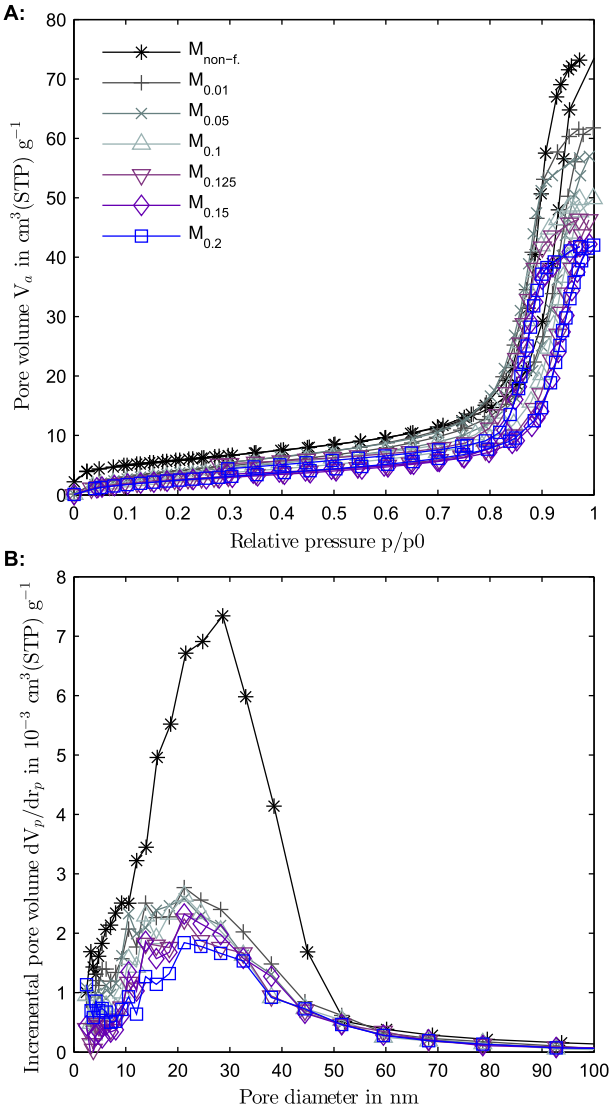

Fig. 3. Exemplary nitrogen adsorption/desorption isotherms (A) and pore size distributions according to Barrett–Joyner–Hallenda model (B) for a non-functionalized and functionalized membranes treated with varying HDTMS concentrations. Sample name subscripts according to the HDTMS concentration (M) used for functionalization.

(> 2%). At small concentrations ($M_{0.01-0.1}$), an increase of the HDTMS molecules in the solution leads to a significant increase in weight loss. However, this dependency stagnates at higher HDTMS concentrations ($M_{0.1-0.2}$). While the total amount of weight loss differs depending on the HDTMS concentration, all curves possess a similar shape. All corresponding DTA signals are very similar (data not shown), showing exothermal reactions for all functionalized membranes when the temperature exceeds 200 °C. In general, the results are in good agreement with measurements performed on non-functionalized and 0.2 M C_{16}-functionalized membranes using TGA and differential scanning calorimetry method as well as total organic and inorganic carbon content tests presented in our previous study [30].

The measured weight loss between 200 and 600 °C obtained from three individual measurements is given in Table 2. Furthermore, the weight loss is recalculated to a functional group density per surface area using the amount of organic compound of the HDTMS molecules (229.5 g mol^{-1}) and the specific surface area determined by nitrogen adsorption/desorption. As already

Table 1
Structural properties of the non-functionalized and C_{16}-functionalized membranes measured by nitrogen adsorption/desorption. Sample name subscripts according to the HDTMS concentration (M) used for functionalization.

Sample name	Specific surface area in $m^2\ g^{-1}$ (BET)	Open porosity in %	Mean pore diameter in nm (BJH)
$M_{non-f.}$	21.17 ± 0.40	37.86 ± 2.21	26.07 ± 2.23
$M_{0.01}$	16.83 ± 0.26	34.69 ± 0.13	21.23 ± 0.00
$M_{0.05}$	15.10 ± 1.04	32.21 ± 0.80	21.23 ± 0.00
$M_{0.1}$	12.21 ± 1.28	30.16 ± 0.47	21.23 ± 0.00
$M_{0.125}$	10.95 ± 0.19	28.75 ± 0.03	19.80 ± 2.02
$M_{0.15}$	10.95 ± 0.88	27.91 ± 1.03	21.23 ± 0.00
$M_{0.2}$	11.22 ± 0.63	26.73 ± 0.47	22.40 ± 1.78

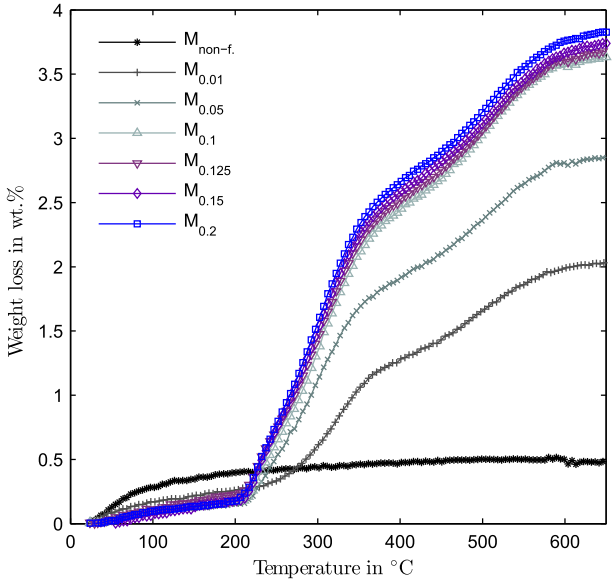

Fig. 4. Exemplary measurements of weight loss determined by TGA of functionalized membranes with varying HDTMS concentration (M) in the stock solution indicated by the subscripts in the sample names.

Table 2
Alkyl-chain density obtained from TGA for samples functionalized with different HDTMS concentrations. Sample name subscripts according to the HDTMS concentration (M) used for functionalization.

Sample name	Weight loss in wt%	Alkyl-chain density	
		In mmol m^{-2}	In groups nm^{-2}
$M_{non-f.}$	0.13 ± 0.03	–	–
$M_{0.01}$	1.58 ± 0.03	3.25 ± 0.01	1.96 ± 0.01
$M_{0.05}$	2.64 ± 0.16	5.44 ± 0.23	3.28 ± 0.14
$M_{0.1}$	3.28 ± 0.08	6.74 ± 0.04	4.06 ± 0.02
$M_{0.125}$	3.3 ± 0.04	6.8 ± 0.04	4.1 ± 0.03
$M_{0.15}$	3.34 ± 0.02	6.88 ± 0.09	4.14 ± 0.05
$M_{0.2}$	3.43 ± 0.01	7.07 ± 0.11	4.25 ± 0.06

indicated by Fig. 4, the weight loss increases rapidly within relatively low applied HDTMS concentrations ($M_{0.01-0.1}$) and stagnates at higher concentrations ($M_{0.1-0.2}$). Based on the weight loss determined by TGA, the calculated C_{16}-chain density on the membrane surface varies between 2 and 4 groups per nm^2.

3.2. Single gas permeation measurements

To investigate the influence of the alkyl-chain density on the membrane surface on the gas transport, gas permeation measurements are carried out under isothermal conditions using Ar, N_2 and CO_2. Fig. 5 shows the results for permeation measurements performed at 20 °C and 80 kPa dead-end pressure. In Fig. 5A the dimensionless molar flow rate is plotted against the dimensionless pressure difference according to Equation (4). For each membrane type indicated by different colors, three consecutive measurements for Ar (◊), N_2 (Δ) and CO_2 (○) are shown. The standard deviations include the errors for temperature, membrane thickness, membrane area, pore diameter and porosity based on the propagation of uncertainty. Especially noticeable for the non-functionalized structures, the most significant impact on the standard deviation are caused by pore size, porosity and membrane surface area and thickness. The deviations deriving from the gas permeation measurements are comparably small. All membrane types show a linear behavior of the gas flow depending on the pressure drop. However, the higher the C_{16}-chain density on the membrane surface, the smaller the slope becomes. After considering the molar mass of the gases, non-functionalized membranes and membranes with a small alkyl-chain density show a gas flow which is independent of gas species.

Fig. 5B shows the slopes obtained by linear regression of the data presented in Fig. 5A depending on the C_{16}-chain density on the membrane surface determined by TGA (see Table 2). The standard deviations presented here include further the deviations from linear regression. Following the Knudsen theory, the slope represents τ^{-2}. It should be pointed out, that in this study the parameter τ^{-2} is not analyzed by means of the conventional definition of tortuosity. This value is used here for interpretation of the measurement results and only serves as an indicator for the mass transport kinetics. It is used to explain effects caused by a C_{16} surface functionalization on the gas flow after considering all membrane parameters such as the change in pore structure according to known relations. As already indicated in Fig. 5A, the slope of linear regression decreases with increasing C_{16}-chain density. Here, a non-linear behavior of τ^{-2} depending on the alkyl-chain density is observed. This is indicated by two linear fits through the data points of the particular region. At very high densities of the surface functionalization ($M_{0.1-0.2}$), the decrease in τ^{-2} is steeper. Furthermore, comparing the slopes of the normalized gas flow for all gas species, CO_2 shows slightly higher values at very high C_{16}-chain densities than Ar and N_2. To analyze the relation between the different gas species, the ideal selectivities for all three gas pair combinations are calculated according to Equation (1). Fig. 6 shows the resulting selectivities, namely N_2/Ar (A), Ar/CO_2 (B) and N_2/CO_2 (C) again depending on the C_{16}-chain density per surface area (see Table 2). The non-functionalized membranes show ideal selectivities in agreement to the Knudsen theory (see Equation (3)) represented by the dashed lines for all gas pairs. Similar results are obtained for membranes possessing low alkyl-chain densities ($M_{0.01-0.05}$). However, increasing the number of C_{16}-chains on the surface of the membranes towards high values of around 4 groups per nm^2 leads to a deviation of the ideal selectivities from the Knudsen relation ($M_{0.1-0.2}$). Especially noticeable is the effect on

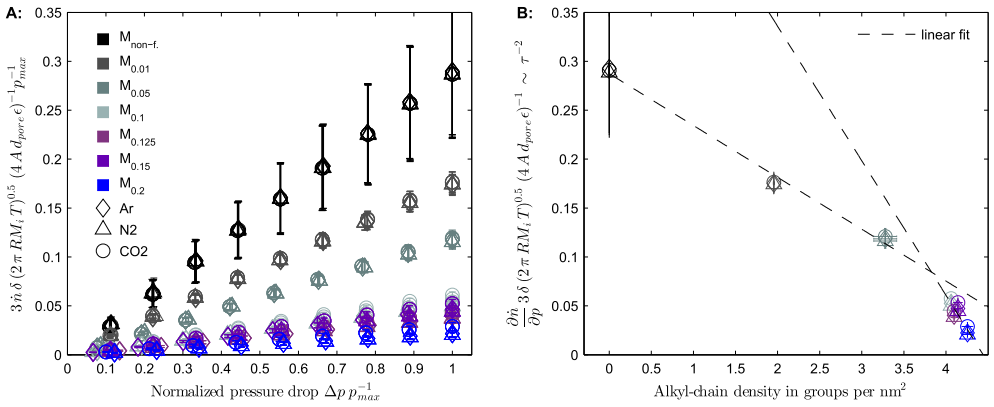

Fig. 5. Dimensionless gas flow versus dimensionless pressure drop (A). Part B shows the slope of linear regression of the data presented in (A) depending on the alkyl-chain density determined by TGA. The slope represents τ^{-2} according to the Knudsen theory. Results are obtained from single gas permeation measurements at 20 C◦ and 80 kPa dead-end pressure.

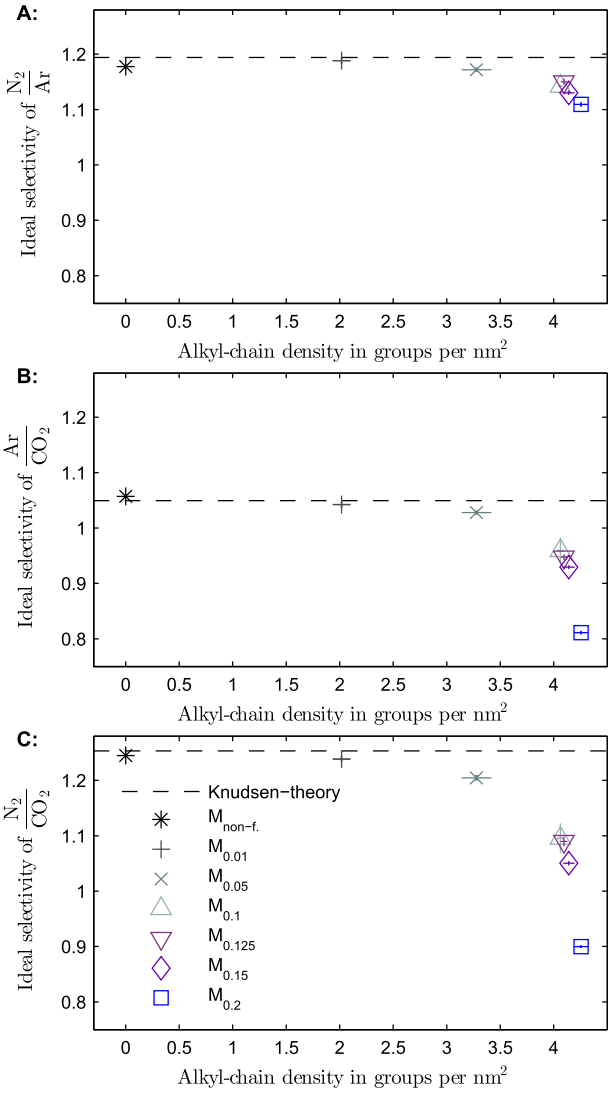

Fig. 6. Ideal selectivities of the non-functionalized and C_{16}-functionalized membranes depending on the alkyl-chain density determined by TGA. The dashed black line represents the Knudsen selectivity proposed by the Knudsen theory. Results are obtained from single gas permeation measurements at 20 C◦ and 80 kPa dead-end pressure.

the selectivity of both inert gases N_2/Ar which decreases at high C_{16}-chain densities. Nevertheless, the ideal selectivities regarding CO_2 are affected to a greater extent, where the highest deviations are obtained for N_2/CO_2.

3.3. Modeling of the alkyl-chain distance

To analyze and understand the influence of the C_{16}-chain density on the gas flow characteristics, the distances between alkyl-chains depending on their density is theoretically calculated by a random distribution approach. Fig. 7 shows the mean distance between the C_{16}-chains on the membrane surface depending on the C_{16}-chain density as a result from theoretical calculations. For low densities (< 2 groups nm2−), the mean distance between the functional molecules on the surface is several nanometers large. In turn, for high densities (>4 groups nm^{-2}), the mean distance drops into the sub nanometer range, specifically, for a density of 4 groups per nm^2 the mean distance is calculated to be 0.73 ± 0.14 nm.

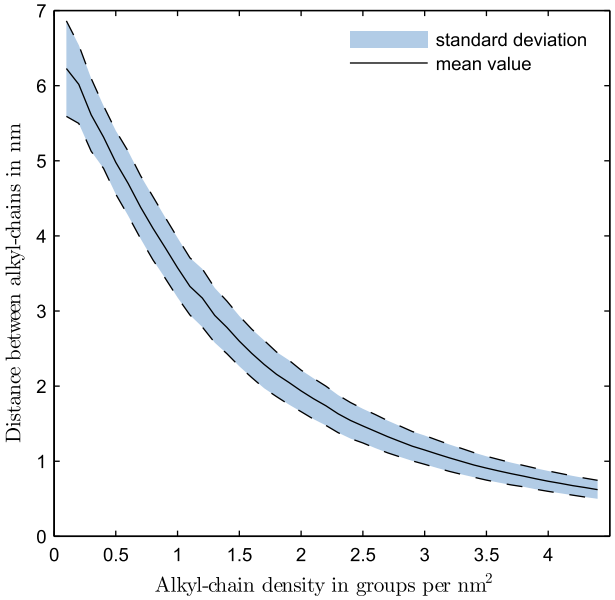

Fig. 7. Distance between the C_{16}-chains in nm depending on the alkyl-chain density on the membrane surface as a result of the theoretical model.

4. Discussion

4.1. Structural properties and surface functionalization

To ensure comparability of the porous structures before and after functionalization with HDTMS, nitrogen adsorption/desorption isotherms are carried out. The results show a decrease in porosity and mean pore diameter when functionalized with alkyl-chains. While the open porosity decreases with an increase in HDTMS concentration, the mean pore diameter is similar for all functionalized membranes $M_{0.01}$ to $M_{0.2}$. Fig. 8 illustrates the capillary condensation of nitrogen in pore structures with different alkyl-chain densities aiming to explain the decrease in pore diameter. A homogeneous distribution of the C_{16}-chains on the pore walls of the membrane surface as well as mono-layer formation with straight oriented alkyl-chains is assumed. Accordingly, a relatively small amount of molecules will already lead to a decrease in pore radius by the length of the C_{16}-chains ($M_{0.01}$). Additional alkyl-chains at higher densities($M_{0.05-0.2}$) will fill up the free space between the existing chains on the membrane surface. This leads to a decrease in the amount of nitrogen molecules which can be introduced into the porous structure, i.e. resulting in a decrease in open porosity while the pore radius will remain the same. The measurements show that the mean pore radius is decreased by around 2.4 nm due to the C_{16}-functionalization which indicates a mono-layer formation given by the size of the C_{16}-chains of around 2.3 nm assuming straight orientation of the alkyl chains from the pore wall surface.

Fig. 9 combines the decrease in open porosity determined by nitrogen adsorption/desorption and the alkyl-chain density obtained by TGA. Depending on the HDTMS concentration of the stock solution, the open porosity decreases and the C_{16}-chain density increases. For high concentrations ($M_{0.125-0.2}$), the open porosity decreases by a high content, whereas the increase in C_{16}-chain density is rather small. Following the illustrative condensation model presented in Fig. 8, introducing C_{16}-chains with a low density ($M_{0.01-0.1}$) will lead to a decrease in open porosity. Incrementally added alkyl-chains ($M_{0.125-0.2}$) will fill and eventually close the gaps between the already immobilized C_{16}-chains. Closing the gaps will result in a high decrease in open porosity caused by a comparably small amount of additional alkyl-chains, which can be observed in Fig. 9. For some polar surface functionalizations, for example silanes showing amino-groups, it is assumed that they are able to form multi-layers when the functional groups react with each other or the silane-hydroxyl groups, which eventually results in pore blocking [41]. Of course, pore blocking as well as multi-layer formation may be a possible explanation for the decrease in open porosity here as well. But in this case, the hydrolyzed HDTMS molecules present a structure similar to amphiphilic fatty acids with a hydrophobic tail and a hydrophilic head, which interacts with a hydrophilic membrane surface obtained by acicid hydroxylation (activation). Accordingly, a mono-layer formation similar to a self assembly of lipids on an oil-water interface is more likely than a multi-layer formation or extensive pore blocking. An additional random test with a membrane functionalized using a 0.3 M HDTMS solution showed no further decrease of open porosity or pore diameter nor an increase in weight loss which supports this assumption (data not shown). Therefore, it is assumed that $M_{0.2}$ possesses a functional group density close to the maximum possible surface coverage. This is supported by the alkyl-chain density values obtained from TGA of around 4.3 groups per nm^2 (see Table 2). In comparison, literature values obtained from water adsorption show a hydroxyl group density of 8–15 groups nm^{-2} on ZrO_2 [42–44]. Taking into account the size of a HDTMS molecule compared to water, 4.3 groups nm^{-2} is considered rather high and close to the maximum possible packing density due to steric reasons, assuming that one HDTMS molecule can covalently bond to one hydroxyl group.

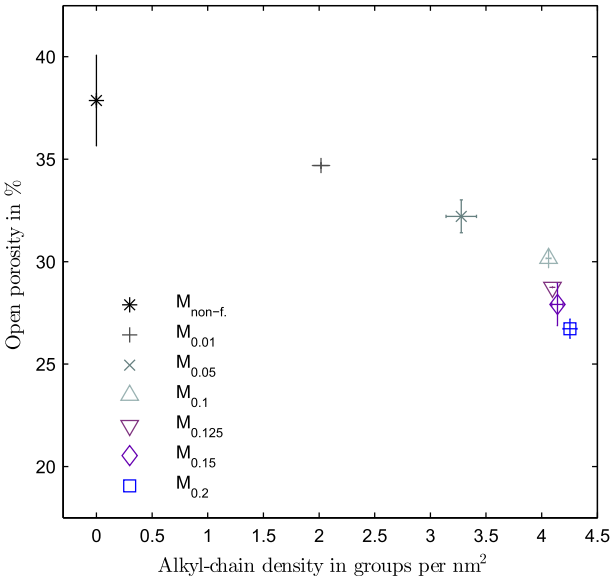

Fig. 9. Open porosity determined by nitrogen adsorption/desorption versus C_{16}-chain density obtained from TGA.

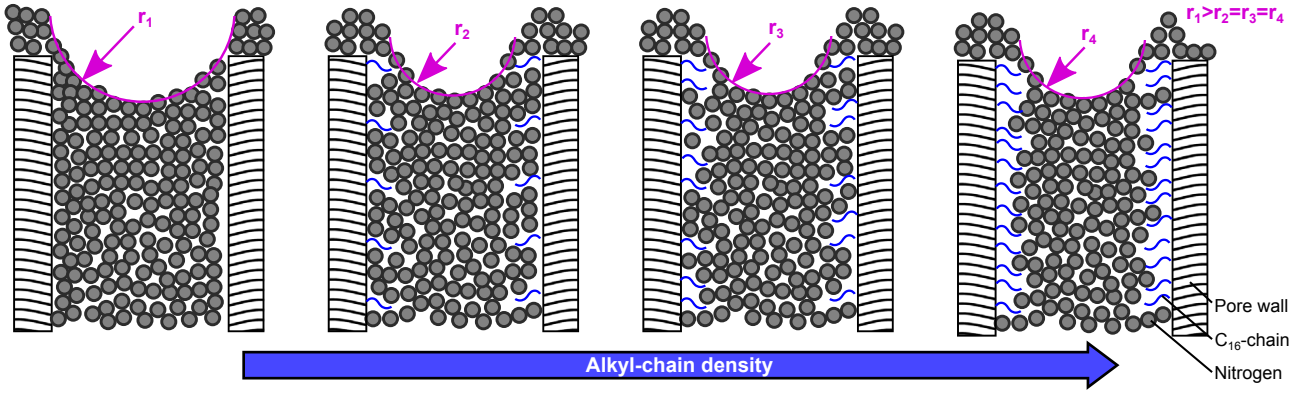

Fig. 8. Schematical illustration of the capillary condensation during nitrogen adsorption/desorption on membranes with different alkyl-chain densities.

4.2. Gas transport through alkyl-functionalized structures

Gas permeation measurements are carried out to investigate the influence of the C_{16}-chain density on the gas flow behavior. The measurements reveal a linear dependency between gas flow and pressure drop which indicates that the predominant gas transport mechanism is Knudsen diffusion without any influence of viscous flow (see Fig. 5A). Applying the Knudsen relation, especially regarding temperature and molar mass of the gas reveals good agreement with the Knudsen theory because the normalized flow is independent of gas species. Nevertheless, linear regression of the permeation data shows a decreasing slope (τ^{-2}) with increasing C_{16}-chain density (see Fig. 5B). τ^{-2} first linearly decreases with increasing alkyl-chain density ($M_{non.-f-0.05}$) until ~4 groups nm^{-2} after which, the decrease seems to follow a different trend ($M_{0.1-0.2}$). In summary, for high C_{16}-chain densities ($M_{0.2}$) the normalized flow is about one order of magnitude lower which is consistent with literature data [20–22,24–27,29,45]. The decrease in gas flow is usually explained by the decrease in porosity and pore size. Clearly, this cannot be suggested as a reason in this case, because the decrease in porosity and pore diameter has already been accounted for by normalizing the gas flow according to Equation (4). This equation describes the porous structure as a resistance to the gas flow depending on porosity, pore diameter and tortuosity. Being aware of the variety of proposed tortuosity relations [46–49] also dependent on porosity, the measurement results lead to the conclusion that the resistance is not solely defined by the pore morphology but also linked to the functional group density. This suggests that the resistance to the gas flow is a combination of a pore resistance characterized by structural proportions and an additional surface resistance, induced by functional molecules immobilized on the surface. This surface resistance seems to be negligible for non-functionalized "smooth surfaces" but affects the gas flow if the surface is "rough" as in the case of a surface functionalization. Furthermore, its impact seems to depend on the functional group density with strong effects present at high functional group densities ($M_{0.1-0.2}$). One possible explanation is related to the altered surface topography caused by the long alkyl-chains. The observed relation between the C_{16}-chain density and the reduction of gas flow supports this hypothesis. The Knudsen relation assumes smooth surfaces and a diffuse desorption in random directions where the probability is proportional to the angle relative to the surface normal vector [50]. Grafting long alkyl-chains onto the surface renders these assumptions inapplicable. In principle, instead of facing a surface similar to a desert, the gas molecules face an environment similar to a savanna ($M_{0.01-0.05}$). The "free" Knudsen diffusion is still possible, because the distance between the "trees" is rather large. Still, the desorption angle is limited in certain directions. Accordingly, the gas flow is reduced due to longer diffusion paths for the gas molecules through the porous structures. With increasing the C_{16}-chain density ($M_{0.1-0.2}$), –the savanna turns into a dense forest, where the distances between the "trees" are eventually within the order of magnitude of the gas molecules (see Fig. 7). At this point, a "free" Knudsen diffusion is prohibited in almost all directions which reduces the diffusion to a great extent and may even force the molecules to diffuse through the forest without desorption into the free pore volume. Of course, the alkyl-chains on the pore walls are not strictly perpendicular to the surface. Most likely they will be bent and rotated instead of showing a straight alignment and they will be in constant movement when the temperature exceeds the freezing point of the functional layer. Consequently, the temperature will have a direct impact on the movement of the alkyl-chains and, in turn, also on the gas transport properties. The investigation of the influence of temperature on the gas transport properties is not focused here but it is of high interest for further research. Analyzing the ideal selectivities in Fig. 6 reveals a similar behavior and supports this hypothesis. Here, the ideal selectivities follow the Knudsen selectivity for low C_{16}-chain densities ($M_{non-f.-0.05}$), suggesting that the governing transport mechanism is dominated by Knudsen diffusion. Nevertheless, for high alkyl-chain densities of > 4 groups nm^{-2} ($M_{0.1-0.2}$), the ideal selectivities begin to deviate from the Knudsen selectivity. All gas species which are used in this work are non-polar. They differ in "size", number of atoms and therefore mass, atom/electron configurations and therefore quadrupole moment (q~*Ar* 0 Cm^2, q~*N*2 $-4.65 \cdot 10^{-40}$ Cm^2, q~*CO*2 $-14.27 \cdot 10^{-40}$ Cm^2 [51]). In general, for pore sizes and Knudsen numbers investigated within this work, only the molecular mass of the gas should affect the gas flow and selectivity according to the laws of Knudsen diffusion (see Equations (2)–(4)). Besides that, the two other possible parameters are "size" and quadrupole moment. The quadrupole moment is very closely related to the atom/electron configuration and therefore related to the adsorption behavior of the gas species. We can show that the isosteric heat of adsorption for CO_2 (highest q value) significantly decreases from 28 to around 9 kJ mol^{-1} due to the alkyl-chains (data not shown). This indicates that adsorptive interactions with the material surface decreases significantly which leads to the hypothesis that the change in selectivity for high functionalization densities is related to the different kinetic diameters of the gas molecules. Fig. 7 theoretically shows that for very high densities of functional molecules (> 4 groups nm^{-2}), the mean distance between the alkyl-chains gets within the order of magnitude of the molecular diameter of the gases. In this case, different molecular sizes will have an impact on the gas diffusion within the functionalization layer. Following this assumption, larger gas molecules will face a higher resistance due to a reduced mobility than smaller ones which will result in an effect comparable to molecular sieving. The three investigated gases possess kinetic diameters of d_{N_2}=360 p.m., d_{Ar}=340 p.m. and d_{CO_2}=330 p.m. [39]. Accordingly, N_2 will face a higher resistance than Ar due to the larger molecular diameter, in turn the selectivity N_2/Ar will decrease when the distance between the alkyl-chains gets very small (i.e. high functional group density, see Fig. 6). The same selectivity decrease is observed for the selectivities regarding CO_2 which can be explained in the same way. The higher deviations for Ar/CO_2 and N_2/CO_2 may be due to the linear shape of the CO_2 molecule where the diameter perpendicular to the longitudinal axis is significantly smaller than the length. Based on simulations, Yu et al. showed that the CO_2 molecule orients with its longitudinal axis parallel to an alkyl-chain for a minimal energy configuration [52]. Assuming this orientation, the effective molecular diameter of CO_2 will be significantly smaller than 330 p.m. which will lead to a smaller resistance and a higher deviation from the Knudsen selectivities when compared to the flow of other, more spherical gas species such as Ar or N_2. Usually, surface diffusion and viscous flow are the most obvious transport mechanisms causing a deviation from the Knudsen theory. Viscous flow can be excluded due to the linear flow rate as well as the relation of the dynamic viscosity of the gas species (CO_2< N_2< Ar) which will cause a different effect on the selectivities. Surface diffusion seems to be unlikely in this case as well. In general, surface diffusion is understood as a transport mechanism, which results from a selective adsorption and diffusion, increasing the flow of a specific gas species. Here, the diffusion resistance is significantly increased for all gas species, where slight differences are observed depending on the molecular size of the gas. Furthermore, alkyl-functionalizations are known to facilitate surface diffusion of apolar gas species such as hydrocarbons with little affect on polar gases such as CO_2 [25,26,53]. A more appropriate description of the mechanism will be analogue to the molecular sieving effect.

5. Conclusion

Model mesoporous structures are prepared using a yttria-stabilized zirconia nanopowder to investigate the impact of the surface functionalization density of alkyl-chains (C_{16}-chains) on the gas diffusion in mesopores. The inorganic non-functionalized membrane structures feature a mono-modal pore size distribution with a mean pore diameter of 26 nm. Solutions containing different concentrations of the surface functionalization molecules (HDTMS) are used to achieve mesoporous membranes with different alkyl-group densities on the surface. After functionalization, the pore diameter is reduced to around 21 nm due to the C_{16}-chains immobilized on the membrane surface. While the reduction in pore size is found to be independent from functional group density, the open porosity decreases with increasing C_{16}-chain density. Assuming that the HDTMS molecules are distributed homogeneously on the membrane surface, an increase in the alkyl-group density will result in filling the space between the immobilized chains. Therefore, results obtained from nitrogen adsorption/desorption measurements show a decrease in open porosity with increasing functional group density whereas the determined pore diameter remains constant. To determine the effect of the functional group density on the gas diffusion behavior, single gas permeation measurements are performed using Ar, N_2 and CO_2. Gas diffusion in mesopores usually occurs according to the laws of Knudsen diffusion which is confirmed for mesoporous structures without surface functionalization. In contrast, membranes with a alkyl-chain functionalization show gas diffusion kinetics where the gas flow decreases with increasing chain density on the membrane surface. It is proposed, that relatively long C_{16}-chains (~ 2.3 nm) attached to the surface lead to an increased resistance for the Knudsen diffusion because the diffuse desorption of the gas molecules is limited to a certain extent by the chains acting as steric barriers. For high functional group densities (> 4 groups nm^{-2}) where the mean distance of the chains is in the order of magnitude of the size of the gas molecules, the gas flow is reduced disproportional. At the same time the ideal selectivities of the functionalized membranes begin to deviate from Knudsen selectivity. The observed deviations in selectivity are not considered to be related to surface diffusion, which is defined by selective adsorption and diffusion increasing the flow of a specific gas species. Here, the selective mechanism is caused by retention of the gas molecules depending on their size which is better described by an effect similar to molecular sieving. It is proposed, that the different molecular sizes of the gases gain importance when the mean distance between the surface functional groups is in the range of the gas molecular diameters. This leads to a size dependent separation effect within the functional alkyl-layer with a higher retention for large molecules compared to smaller gas species. Furthermore, the results can lead to the conclusion, that the size of the surface functional molecules play a significant role for the gas transport properties. Following this assumption, the "molecule of choice" for a specific application does not solely depend on its functional group type, but also on its size. Accordingly, molecules for a gas separation membrane aiming at enhancing the surface selective flow should be as small as possible whereas a gas chromatography application may benefit from long functional molecules, maximizing the retention effect. Further research may include the investigation of temperature effects on the gas transport properties within these structures. The alkyl-chains are not oriented in a perfect straight manner from the surface, they will rotate, bent and move depending on the applied temperature. This may lead to an increased interaction between surface functional groups and gas molecules which potentially has an effect on the gas flow and/or the ideal selectivities.

Acknowledgements

This work was supported by the German Research Foundation (DFG) within the Research Training Group GRK 1860 "Micro-, meso- and macroporous nonmetallic Materials: Fundamentals and Applications" (MIMENIMA). The support of M. Hoog Antink from the University of Bremen for the fruitful discussions and the critical feedback which helped to improve this work is gratefully acknowledged. Furthermore, we thank T. Kühn from the University of Bremen for all the support in the laboratory.

References

[1] W. He, W. Lv, J.H. Dickerson, Gas Transport in Solid Oxide Fuel Cells, Springer Briefs in Energy, Springer International Publishing, 2014, http://dx.doi.org/10.1007/978-3-319-09737-4_2. http://dx.doi.org/10.1007/978-3-319-09737-4_2.

[2] M.-O. Coppens, A nature-inspired approach to reactor and catalysis engineering, Curr. Opin. Chem. Eng. 1 (3) (2012) 281–289, http://dx.doi.org/10.1016/j.coche.2012.03.002. http://dx.doi.org/10.1016/j.coche.2012.03.002.

[3] J. Baxter, Z. Bian, G. Chen, D. Danielson, M.S. Dresselhaus, A.G. Fedorov, T.S. Fisher, C.W. Jones, E. Maginn, U. Kortshagen, A. Manthiram, A. Nozik, D.R. Rolison, T. Sands, L. Shi, D. Sholl, Y. Wu, Nanoscale design to enable the revolution in renewable energy, Energy Environ. Sci. 2 (2009) 559–588, http://dx.doi.org/10.1039/B821698C. http://dx.doi.org/10.1039/B821698C.

[4] V. Berezkin, J. de Zeeuw, Capillary gas adsorption chromatography, Hüthig Heidelberg, 1996. ISBN 3-7705-2307-4.

[5] D.Y. Leung, G. Caramanna, M.M. Maroto-Valer, An overview of current status of carbon dioxide capture and storage technologies, Renew. Sustain. Energy Rev. 39 (2014) 426–443, http://dx.doi.org/10.1016/j.rser.2014.07.093. http://dx.doi.org/10.1016/j.rser.2014.07.093.

[6] M.E. Boot-Handford, J.C. Abanades, E.J. Anthony, M.J. Blunt, S. Brandani, N. Mac Dowell, J.R. Fernandez, M.-C. Ferrari, R. Gross, J.P. Hallett, R.S. Haszeldine, P. Heptonstall, A. Lyngfelt, Z. Makuch, E. Mangano, R.T.J. Porter, M. Pourkashanian, G.T. Rochelle, N. Shah, J.G. Yao, P.S. Fennell, Carbon capture and storage update, Energy Environ. Sci. 7 (2014) 130–189, http://dx.doi.org/10.1039/C3EE42350F. http://dx.doi.org/10.1039/C3EE42350F.

[7] B. Besser, H.A. Tajiri, G. Mikolajczyk, J. Möllmer, T.C. Schumacher, S. Odenbach, R. Gläser, S. Kroll, K. Rezwan, Hierarchical porous zeolite structures for pressure swing adsorption applications, ACS Appl. Mater. Interfaces 8 (5) (2016) 3277–3286, http://dx.doi.org/10.1021/acsami.5b11120. http://dx.doi.org/10.1021/acsami.5b11120.

[8] A.F. Ismail, K.C. Khulbe, T. Matsuura, Gas Separation Membranes: Polymeric and Inorganic, Springer International Publishing, 2015, http://dx.doi.org/10.1007/978-3-319-01095-3.

[9] H. Verweij, Ceramic membranes: morphology and transport, J. Mater. Sci. 38 (23) (2003) 4677–4695, http://dx.doi.org/10.1023/A:1027410616041. http://dx.doi.org/10.1023/A:1027410616041.

[10] A. Seidel-Morgenstern, Membrane Reactors, Wiley-VCH, 2010.

[11] D.M. Ruthven, W. DeSisto, S. Higgins, Diffusion in a mesoporous silica membrane: validity of the knudsen diffusion model, Chem. Eng. Sci. 64 (13) (2009) 3201–3203, http://dx.doi.org/10.1016/j.ces.2009.03.049. http://dx.doi.org/10.1016/j.ces.2009.03.049.

[12] R. Krishna, J. van Baten, An investigation of the characteristics of maxwell-stefan diffusivities of binary mixtures in silica nanopores, Chem. Eng. Sci. 64 (5) (2009) 870–882, http://dx.doi.org/10.1016/j.ces.2008.10.045. http://dx.doi.org/10.1016/j.ces.2008.10.045.

[13] W.V. Chiu, I.S. Park, K. Shqau, J.C. White, M.C. Schillo, W.S.W. Ho, P.K. Dutta, H. Verweij, Post-synthesis defect abatement of inorganic membranes for gas separation, J. Membr. Sci. 377 (1–2) (2011) 182–190, http://dx.doi.org/10.1016/j.memsci.2011.04.047. http://www.sciencedirect.com/science/article/pii/S0376738811003127.

[14] H. Meinema, R. Dirrix, H. Brinkman, R. Terpstra, J. Jekerle, P. Kösters, Ceramic membranes for gas separation - recent developments and state of the art, Interceram 54 (2005) 86–91.

[15] W.J. Koros, R. Mahajan, Pushing the limits on possibilities for large scale gas separation: which strategies? J. Membr. Sci. 175 (2) (2000) 181–196, http://dx.doi.org/10.1016/S0376-7388(00)00418-X. http://www.sciencedirect.com/science/article/pii/S037673880000418X.

[16] A.D. Wiheeb, M.A. Ahmad, M.N. Murat, J. Kim, M.R. Othman, Identification of molecular transport mechanisms in micro-porous hydrotalcite-silica membrane, Transp. Porous Media 104 (1) (2014) 133–144, http://dx.doi.org/10.1007/s11242-014-0324-5. http://dx.doi.org/10.1007/s11242-014-0324-5.

[17] Y. Zheng, M. Qi, R. Fu, Graphitic carbon nitride as high-resolution stationary phase for gas chromatographic separations, J. Chromatogr. A 1454 (2016) 107–113. http://www.sciencedirect.com/science/article/pii/S002196731630680X.

[18] Y. Zhang, J. Sunarso, S. Liu, R. Wang, Current status and development of membranes for co2/ch4 separation: a review, Int. J. Greenh. Gas Control 12 (2013) 84–107, http://dx.doi.org/10.1016/j.ijggc.2012.10.009. http://dx.doi.org/10.1016/j.ijggc.2012.10.009.

[19] J. Adewole, A. Ahmad, S. Ismail, C. Leo, Current challenges in membrane separation of co2 from natural gas: a review, Int. J. Greenh. Gas Control 17 (2013) 46–65, http://dx.doi.org/10.1016/j.ijggc.2013.04.012. http://dx.doi.org/10.1016/j.ijggc.2013.04.012.

[20] C. Leger, H.D.L. Lira, R. Paterson, Preparation and properties of surface modified ceramic membranes. part iii. gas permeation of 5 nm alumina membranes modified by trichloro-octadecylsilane, Journal of Membrane Science 120 (2) (1996) 187–195. http://www.sciencedirect.com/science/article/pii/0376738896001433.

[21] D. Stoltenberg, A. Seidel-Morgenstern, An attempt to alter the gas separation of mesoporous glass membranes by amine modification, Microporous Mesoporous Mater. 154 (2012) 148–152, http://dx.doi.org/10.1016/j.micromeso.2011.11.013. http://dx.doi.org/10.1016/j.micromeso.2011.11.013.

[22] S. Suzuki, S.B. Messaoud, A. Takagaki, T. Sugawara, R. Kikuchi, S.T. Oyama, Development of inorganic-organic hybrid membranes for carbon dioxide/methane separation, J. Membr. Sci. 471 (2014) 402–411. http://www.sciencedirect.com/science/article/pii/S0376738814006450.

[23] D. Wang, H. Shakeel, J. Lovette, G.W. Rice, J.R. Heflin, M. Agah, Highly stable surface functionalization of microgas chromatography columns using layer-by-layer self-assembly of silica nanoparticles, Anal. Chem. 85 (17) (2013) 8135–8141, http://dx.doi.org/10.1021/ac401080u. http://dx.doi.org/10.1021/ac401080u.

[24] A. Javaid, M.P. Hughey, V. Varutbangkul, D.M. Ford, Solubility-based gas separation with oligomer-modified inorganic membranes, J. Membr. Sci. 187 (1–2) (2001) 141–150. http://www.sciencedirect.com/science/article/pii/S0376738801003416.

[25] R.P. Singh, J.D. Way, S.F. Dec, Silane modified inorganic membranes: effects of silane surface structure, J. Membr. Sci. 259 (1–2) (2005) 34–46, http://dx.doi.org/10.1016/j.memsci.2005.03.004. http://www.sciencedirect.com/science/article/pii/S0376738805001973.

[26] K. Kuraoka, Y. Chujo, T. Yazawa, Hydrocarbon separation via porous glass membranes surface-modified using organosilane compounds, J. Membr. Sci. 182 (1–2) (2001) 139–149, http://dx.doi.org/10.1016/S0376-7388(00)00559-7. http://www.sciencedirect.com/science/article/pii/S0376738800005597.

[27] A. Lindbråthen, M.-B. Hägg, Glass membranes for purification of aggressive gases: Part ii. adsorption measurements and diffusion coefficient estimations, J. Membr. Sci. 259 (1–2) (2005) 154–160. http://www.sciencedirect.com/science/article/pii/S037673880500308X.

[28] A. Lindbråthen, M.-B. Hägg, Glass membranes for purification of aggressive gases: Part i: permeability and stability, J. Membr. Sci. 259 (1–2) (2005) 145–153. http://dx.doi.org/10.1016/j.memsci.2005.03.056. http://www.sciencedirect.com/science/article/pii/S0376738805003078.

[29] Y. Sakamoto, K. Nagata, K. Yogo, K. Yamada, Preparation and CO_2 separation properties of amine-modified mesoporous silica membranes, Microporous Mesoporous Mater. 101 (1–2) (2007) 303–311, http://dx.doi.org/10.1016/j.micromeso.2006.11.007. http://dx.doi.org/10.1016/j.micromeso.2006.11.007.

[30] B. Besser, T. Veltzke, J.A. Dreyer, J. Bartels, M. Baune, S. Kroll, J. Thöming, K. Rezwan, A comparative experimental study on the deviation of the ideal selectivity in hdtms-functionalized and untreated ceramic structures with pores in the upper mesoporous range, Microporous Mesoporous Mater. 217 (0) (2015) 253–261. http://www.sciencedirect.com/science/article/pii/S1387181115003753.

[31] J. Werner, B. Besser, C. Brandes, S. Kroll, K. Rezwan, Production of ceramic membranes with different pore sizes for virus retention, J. Water Process Eng. 4 (2014) 201–211, http://dx.doi.org/10.1016/j.jwpe.2014.10.007. http://dx.doi.org/10.1016/j.jwpe.2014.10.007.

[32] J. Bartels, M.N. Souza, A. Schaper, P. Árki, S. Kroll, K. Rezwan, Amino-functionalized ceramic capillary membranes for controlled virus retention, Environ. Sci. Technol. (2016), http://dx.doi.org/10.1021/acs.est.5b05124. http://dx.doi.org/10.1021/acs.est.5b05124.

[33] S. Kroll, M.O.C. de Moura, F. Meder, G. Grathwohl, K. Rezwan, High virus retention mediated by zirconia microtubes with tailored porosity, J. Eur. Ceram. Soc. 32 (16) (2012) 4111–4120, http://dx.doi.org/10.1016/j.jeurceramsoc.2012.07.026. http://www.sciencedirect.com/science/article/pii/S0955221912004220.

[34] S. Kroll, L. Treccani, K. Rezwan, G. Grathwohl, Development and characterisation of functionalised ceramic microtubes for bacteria filtration, J. Membr. Sci. 365 (1–2) (2010) 447–455. http://www.sciencedirect.com/science/article/pii/S0376738810007568.

[35] S. Kroll, C. Brandes, J. Wehling, L. Treccani, G. Grathwohl, K. Rezwan, Highly efficient enzyme-functionalized porous zirconia microtubes for bacteria filtration, Environ. Sci. Technol. 46 (16) (2012) 8739–8747, http://dx.doi.org/10.1021/es3006496. http://dx.doi.org/10.1021/es3006496.

[36] E.P. Barrett, L.G. Joyner, P.P. Halenda, The determination of pore volume and area distributions in porous substances. i. computations from nitrogen isotherms, J. Am. Chem. Soc. 73 (1) (1951) 373–380, http://dx.doi.org/10.1021/ja01145a126. http://dx.doi.org/10.1021/ja01145a126.

[37] S. Brunauer, P.H. Emmett, E. Teller, Adsorption of gases in multimolecular layers, J. Am. Chem. Soc. 60 (2) (1938) 309–319, http://dx.doi.org/10.1021/ja01269a023. http://dx.doi.org/10.1021/ja01269a023.

[38] T. Veltzke, M. Baune, J. Thöming, The contribution of diffusion to gas microflow: an experimental study, Phys. Fluids 24 (8) (2012), http://dx.doi.org/10.1063/1.4745004. http://dx.doi.org/10.1063/1.4745004.

[39] D. Breck, Crystalline molecular sieves, J. Chem. Educ. (1964) 678–689.

[40] S.W. Sing, Reporting physisorption data for gas/solid systems with special reference to the determination of surface area and porosity, Pure Appl. Chem. 54 (11) (1982) 2201–2218, http://dx.doi.org/10.1351/pac198254112201.

[41] M. Zhu, M.Z. Lerum, W. Chen, How to prepare reproducible, homogeneous, and hydrolytically stable aminosilane-derived layers on silica, Langmuir 28 (1) (2012) 416–423, http://dx.doi.org/10.1021/la203638g. http://dx.doi.org/10.1021/la203638g.

[42] J. Randon, A. Larbot, A. Julbe, C. Guizard, L. Cot, Study of ZrO_2 membrane - aqueous solutions interface, Key Eng. Mater. 61–62 (1992) 495–498. www.scientific.net/kem.61-62.495. http://dx.doi.org/10.4028/www.scientific.net/KEM.61-62.495.

[43] J. Nawrocki, M. Rigney, A. McCormick, P. Carr, Chemistry of zirconia and its use in chromatography, J. Chromatogr. A 657 (2) (1993) 229–282. http://www.sciencedirect.com/science/article/pii/002196739380284F.

[44] J. Nawrocki, P. Carr, M.J. Annen, S. Froeliche, A TGA investigation of hydrated monoclinic zirconia, Anal. Chim. ACTA 327 (3) (1996) 261–266, http://dx.doi.org/10.1016/0003-2670(96)00110-9.

[45] S.B. Messaoud, A. Takagaki, T. Sugawara, R. Kikuchi, S.T. Oyama, Alkylamine–silica hybrid membranes for carbon dioxide/methane separation, J. Membr. Sci. 477 (0) (2015) 161–171. http://dx.doi.org/10.1016/j.memsci.2014.12.022. http://www.sciencedirect.com/science/article/pii/S0376738814009259.

[46] X. Gao, J.C. Diniz da Costa, S.K. Bhatia, Understanding the diffusional tortuosity of porous materials: an effective medium theory perspective, Chem. Eng. Sci. 110 (2014) 55–71, http://dx.doi.org/10.1016/j.ces.2013.09.050. http://dx.doi.org/10.1016/j.ces.2013.09.050.

[47] L. Shen, Z. Chen, Critical review of the impact of tortuosity on diffusion, Chem. Eng. Sci. 62 (14) (2007) 3748–3755. http://www.sciencedirect.com/science/article/pii/S0009250907003144.

[48] S.K. Bhatia, D. Nicholson, Comments on “diffusion in a mesoporous silica membrane: validity of the knudsen diffusion model”, by Ruthven, D.M., et al., Chem. Eng. Sci.. 64 (2009) 3201–3203, Chemical Engineering Science 65 (15) (2010) 4519–4520. http://www.sciencedirect.com/science/article/pii/S0009250910002708.

[49] S.K. Bhatia, D. Nicholson, Some pitfalls in the use of the knudsen equation in modelling diffusion in nanoporous materials, Chem. Eng. Sci. 66 (3) (2011) 284–293.

[50] J. Liu, J. Wei, Knudsen diffusion in channels and networks, Chem. Eng. Sci. 111 (2014) 1–14. http://www.sciencedirect.com/science/article/pii/S0009250914000165.

[51] D.A. Graham, R.E. Imrie, C. Raab, Measurement of the electric quadrupole moments of co2, co, n2, cl2 and bf3, Mol. Phys. 93 (1) (1998) 49–56, http://dx.doi.org/10.1080/002689798169429. http://dx.doi.org/10.1080/002689798169429.

[52] D. Yu, S. Matteucci, E. Stangland, E. Calverley, H. Wegener, D. Anaya, Quantum chemistry calculation and experimental study of CO_2/CH_4 and functional group interactions for the design of solubility selective membrane materials, J. Membr. Sci. 441 (2013) 137–147, http://dx.doi.org/10.1016/j.memsci.2013.03.052. http://dx.doi.org/10.1016/j.memsci.2013.03.052.

[53] S. Higgins, W. DeSisto, D. Ruthven, Diffusive transport through mesoporous silica membranes, Microporous Mesoporous Mater. 117 (1–2) (2009) 268–277, http://dx.doi.org/10.1016/j.micromeso.2008.06.030. http://dx.doi.org/10.1016/j.micromeso.2008.06.030.